Variability of Antarctic Bottom Water at 24.5°N in the Atlantic

E. Frajka-Williams,[1] S. A. Cunningham,[1] H. Bryden[2] and B. A. King[1]

H. Bryden, National Oceanography Centre, University of Southampton Waterfront Campus, European Way, Southampton, SO14 3ZH, UK (h.bryden@noc.soton.ac.uk)

S. A. Cunningham, National Oceanography Centre, University of Southampton Waterfront Campus, European Way, Southampton, SO14 3ZH, UK (scu@noc.ac.uk)

E. Frajka-Williams, National Oceanography Centre, University of Southampton Waterfront Campus, European Way, Southampton, SO14 3ZH, UK (e.williams@noc.ac.uk)

B. A. King, National Oceanography Centre, University of Southampton Waterfront Campus, European Way, Southampton, SO14 3ZH, UK (bak@noc.ac.uk)

[1]National Oceanography Centre,

Southampton, UK.

[2]School of Ocean and Earth Science,

University of Southampton, Southampton,

UK.

Abstract.

A recent hydrographic section at 24.5°N in the Atlantic and six months of observations from a moored array show that Antarctic Bottom Water (AABW), the densest and deepest watermass in the world oceans, has been warming. While Johnson et al., 2008 [@] showed that northward AABW transport at 24.5°N has been declining from 1981–2004, suggesting that the lower cell of the overturning circulation could halt in the near future, estimates from the latest hydrographic section in 2010 indicate a partial recovery of northward AABW transport. From six months of temperature and salinity observations at a deep moored array at 24–26°N, we find that short-term variability between April and November 2009 is of the same magnitude as the changes observed from hydrographic sections between 1981 and 2004. These observations highlight the possibility that transport changes estimated from hydrographic sections may be aliased by short-term variability. The observed AABW transport variability affects present estimates of the upper meridional overturning circulation by ± 0.4 Sv (1 Sv = 10^6 $m^3 s^{-1}$).

1. Introduction

The ocean meridional overturning circulation (MOC) is responsible for a large fraction of the poleward heat transport in the ocean [Trenberth and Caron, 2001, @]. In the Atlantic, it is characterized by northward flowing warm waters near the surface—concentrated in the Gulf Stream at 26°N—and southward flowing cold waters between roughly 1000 and 5000 m—called the North Atlantic Deep Water (NADW). The overturning strength—estimated using the techniques described in Cunningham et al., 2007 [@]—is 18.6±4.7 Sv between April 2004 to March 2009, with a strong annual cycle and subseasonal variability. Below this overturning circulation lies a deeper overturning cell; this lower cell is comprised of northward flowing Antarctic Bottom Water (AABW) at the bottom of the Atlantic which returns with the southward limb of the upper cell in the NADW. In the global context, the lower cell is of the same strength (roughly 20 Sv) as the upper overturning cell, though it carries less heat and only 6 Sv are in the Atlantic [Orsi et al., 1999, @].

Recent observations have shown a warming of AABW both globally [Purkey and Johnson, 2010, @] and in the South Atlantic [Johnson and Doney, 2006, @]. Along the pathway of AABW into the North Atlantic, progressive warming of AABW has been observed in the Vema Channel (at 31–28°S and 39–40°W, Zenk and Morozov, 2007 [@]), though observations further north at the equator and 36°W showed no warming [Limeburner et al., 2005, @]. In the North Atlantic, Johnson et al., 2008 [@] used a number of hydrographic sections to infer warming of AABW in the past several decades. Using four hydrographic sections at 24°N they show relative to 1981, that the northward transport of AABW has been monotonically decreasing through 2004 (hydrographic stations included in Fig. 1c, which shows 2 additional sections).

From the same hydrographic sections, transports of the full MOC were also calculated, and similarly showed a monotonic decrease in the overturning strength on the order of 30% [Bryden et al., 2005, @] suggesting a possible collapse of the MOC. However, estimates of overturning from a moored array by the joint Rapid Climate Change-Will the Atlantic Thermohaline Circulation Halt (RAPID-WATCH)/Meridional Overturning Circulation and Heatflux Array (MOCHA) project showed that the subannual variability of the MOC since 2004 encompassed the 30% reduction in strength [Cunningham et al., 2007, @] and the monthly timing of the hydrographic sections in 1981, 1992, 1998 and 2004 corresponded to the peak to trough of the annual cycle of transports [Kanzow et al., 2010, @].

What is the variability of AABW transport? Could the trends inferred by Johnson et al., 2008 [@] be similarly aliased by high frequency variability? To investigate these questions, deep moorings were deployed in the western basin of the North Atlantic as part of the larger RAPID-WATCH/MOCHA mooring array (mooring schematic in Fig. 1a). For the MOC calculation in the array, geostrophic transport per unit depth is estimated across 26°N using the dynamic height profiles from a series of moorings at the western boundary (WB), eastern boundary (EB) and mid-Atlantic ridge (MAR) [Cunningham et al., 2007, @]. However, these moorings only extended down to 4820 dbar. Below 4820 dbar, a fixed profile of transport per unit depth is used to represent AABW transport, summing to roughly 2 Sv [Kanzow et al., 2010, @] (updated through April 2009 in Fig. 1b). In 2009, two additional deep moorings were added below 4820 dbar to estimate the variability missed between 70°W and 52°W and deeper than 5100 dbar. In §2, we describe the data and methodology. In §3 we examine the short-term variability of transport and temperature fluctuations, from the mooring array. In §4, we estimate transport and warming from the hydrographic sections—including a recent 2010 repeat of the 24°N hydrographic section [King, B. A., 2011, @]—to put the mooring results in context and to revisit the calculation of Johnson et al., 2008 [@]. We conclude with a discussion of the impacts of these findings on the MOC and our knowledge about the global overturning circulation.

2. Data and Methods

2.1. Moored array

Moorings used in this analysis are part of the RAPID-WATCH/MOCHA (hereafter referred to as RAPID) array at 24–28°N in the Atlantic (See Fig. 1a & c for mooring positions). The array is used to estimate several components of the MOC including geostrophic transport between end point dynamic height moorings and absolute transport in the western boundary region from current meter arrays. When combined with the Gulf Stream transport through the Florida Straits and Ekman transports estimated from satellite wind products, these produce a meridional overturning streamfunction at 26°N every 12 hours. (See Rayner et al, 2011 [@] for a review.)

In this paper, we use the data from the two newly added deep moorings as well as two neighboring tall moorings, between 72°W and 49°W, between Florida and the mid-Atlantic ridge. The two deep moorings were WB_6 in the west at 26.49°N and 70.52°W and MAR_0 at the western flank of the MAR at 24.17°N and 52.01°W (Fig. 1a). The tall moorings were instrumented throughout the water column: WB_5 at 26.50°N and

71.98°W, and MAR_1 at 24.16°N and 49.72°W (Fig. 1a). WB_6 is in the abyssal plain, whereas MAR_0 is in a deep canyon of the mid-Atlantic ridge, chosen to have an open connection to the west at depth. WB_6 and MAR_0 were densely instrumented with five MicroCATs (Sea-Bird Electronics, Bellevue, WA, USA), self-logging instruments which measures temperature, conductivity and pressure, from 5100–5600 dbar: WB_6 had four MicroCATs and MAR_0 had five providing a nominal vertical resolution of about 100 m. The high vertical resolution was motivated in part by the previous deep deployment which suffered high instrument loss rates due to flooding. The tall moorings WB_5 and MAR_1 had MicroCATS every 500 dbar near the seabed. MicroCATs measured temperature and conductivity every 30 minutes, and data were subsampled to 12 hours and low-pass filtered with a ten-day filter. Bottom pressure recorders were also deployed, but as only one of the two bottom pressure recorders was successfully recovered, bottom pressure is not used in this study.

MicroCAT temperature, conductivity and pressure are calibrated using a combination of Sea-Bird laboratory calibrations and pre- and post-cruise calibration dips using the vessel-mounted Seabird conductivity-temperature-depth (CTD). The purpose of the dips is to remove any trends due to sensor drift. For pressure, the signal varied due to drift as well as blowdown by large currents. While typical pressure variations due to blowdown were 100–200 dbar at WB_5 near the surface, they were only 30 dbar below 4000 dbar. Pressure drifts were corrected using an exponential–linear fit to the entire record. On WB_6 and MAR_0, pressure drifts of the Paine pressure sensors were quite large—on the order of 20 dbar over the one year deployment, with some drifts towards increasing pressure while others drifted towards decreasing pressure. In addition, two MicroCATs that were deployed adjacent to each other on the rope (separated by less than 1 m vertically) returned initial pressure readings that were 26 dbar apart. In this instance, pressures were adjusted using the relative spacing between instruments and the bottom depth. For WB_6 and MAR_0, the applied corrections ranged from -6 to 26 dbar. For a typical salinity of 34.85 and temperature of 1.8°C at 5100 dbar, a ±5 dbar offset in pressure would result in ±0.0019 offset in salinities, and a ±0.0001 kg m^{-3} offset in density.

We estimate AABW transport between 70.5°W (WB_6) and 49°W (MAR_1) and below 4100 dbar. Since WB_6 and MAR_0 only had instruments below 5000 dbar, the data from WB_5 and MAR_1 are used to extend the transport profiles between 4100 and 5100 dbar (WB) and 5300 dbar (MAR). At the western edge, in comparing temperature and salinity at 72°W and 70.5°W, we found that differences above 4700 dbar are very small (not shown), and so used data from WB_5 at 4620 and 4100 dbar. At the mid-Atlantic ridge, we used data from MAR_1 at 5160, 4640, and 4130 dbar. At the MAR, these estimates neglect transport in the bottom triangle (below 5300 dbar and between MAR_0 and MAR_1). To estimate this error, we calculated transport in the bottom triangles using hydrographic sections. Overall the transport neglected here was 0.0±0.1 Sv (see Table 1). Temperature and salinity profiles at the west and mid-Atlantic ridge are linearly interpolated onto a regular 20 dbar grid before density is calculated. Geostrophic transports are calculated between the two profiles, relative to 4100 dbar. This choice of level-of-no-motion will be justified below from hydrography. Below the deepest common level (5600 dbar), transport profiles are extrapolated to zero at 6300 dbar.

2.2. Hydrographic sections

Six hydrographic sections at 24°N in the Atlantic are used from 1957, 1981, 1992, 1998, 2004 and 2010. Table 2 contains details of the sections, and Fig. 1c shows the tracks. Latitudes at the western and eastern boundaries varied between early and later sections, and the 2010 section followed the Kane Fracture Zone, the deepest path across the MAR in the area (see the non-zonal segment of the red transect between 40 and 55 °W in Fig. 1c). As technology has improved, longitudinal resolution has increased: the 1957 section occupied 38 stations, compared with the 2010 section that occupied 122 stations between 13° and 77°W. The 2010 section also recorded the deepest measurements along the transect, reaching 6851 dbar (See Fig. 2 and Fig. 3).

In order to compare AABW volumes and properties between sections with variable resolution and maximum bottom depths, data are gridded onto a uniform longitude–depth grid. In particular, early sections were sparsely sampled in longitude so that the station separation in 1957 was 162±48 km compared to 55±23 km in 2010. Data from each section is linearly interpolated onto a fine longitudinal grid (1000 points between 77 and 13°W) and a 1 dbar pressure grid. The 2004 section was limited by instrumentation to a maximum bottom depth of 6000 dbar, even though the water depth was closer to 6400 dbar. The 2010 section, for which casts extended to within 10 m of the bottom, shows that profiles of temperature and salinity are well-mixed in the bottom 500 m in water depths greater than 4000 dbar (e.g., standard deviation of temperature less than 0.025°C and of salinity less than 0.003). For all stations with water depths greater than 4000 dbar, temperature and salinity profiles are extended to the bottom depth using the deepest measurements in the profile. Bottom depth is used at 24.5°N, rather than along the track lines, to reduce variations due to latitudinal changes between section occupations. Bottom depth is estimated from ETOPO bathymetry [U. S. Department of Commerce and Atmospheric Administration, 2006, @]. As an example of the effect of filling the profiles on volume estimates, in 2004, roughly 20% of the water colder than 1.8°C is from the filled bottom of the profiles.

Transports at 24°N have been calculated with several combinations of geostrophic reference levels (as described in Lavin et al., 1998 [@]) including 3200 dbar , 4000 dbar, a different reference level in the deep western boundary current region as the rest of the basin, and including a barotropic correction to ensure no net transport across the section. Here we calculate transport profiles from geostrophic meridional velocities using a 4100 dbar zero-velocity reference level for the section east of the deep western boundary current area. This level-of-no-motion minimizes net transport in the eastern basin below the mid-Atlantic ridge (using a ridge depth of 4000 dbar). For the six hydrographic sections, the net eastern basin transport (east of 46°W and below 4000 dbar) was 0.0±0.3 Sv northward. Recent evidence from the RAPID observations suggest that the barotropic velocities are largest in the western boundary region—not uniformly distributed across the entire basin width [Johns et al., 2008, @; Bryden et al., 2009, @]. We can still enforce a mass balance between the geostrophic transport estimates, Ekman, Gulf Stream and Bering Strait transports, but for our purposes, this would be confined to the region west of 70.5°W. Transport values for each year, with the 4100 dbar geostrophic reference level, are given in Table 3. A second set of transport calculations is done with a 3200 dbar reference level, as in Johnson et al., 2008 [@], with no barotropic velocity applied. In this instance as well, it would be possible to apply the barotropic compensation to the west of the AABW transport region.

3. Results: Moorings

3.1. AABW property variability

Temperature variations are typically vertically coherent. In April and May 2009, a large warm anomaly was visible at both mooring sites at WB_6 and MAR_0 (Fig. 4). In such weak stratification, these small temperature changes represent large vertical displacements of isotherms (roughly 150–300 dbar, not shown). A large cooling signal was also observed in September across four of the five instruments on WB_6.

These large warm fluctuations in WB_6 persisted for about three weeks (late April to mid-May) with a peak-to-peak temperature range of over 0.1°C at 5400 dbar (See Fig. 4a). The reverse event in September 2009 was quite brief by comparison (17 Sep–24 Sep). At MAR_0, similar warm fluctuations were seen, both in January 2009 and a larger one in May 2009. The May event appears to be bottom intensified with the sharpest changes at 5500 dbar (about 0.05°C in a couple days, 6 May–8 May).

The data also show a small, longer period warming trend in the deepest MicroCATs on MAR_0 of 0.03°C over the 360 day deployment, calculated as a linear fit to the data (See Fig. 4b). Salinities increased by roughly 0.04 over the same period (not shown). While we cannot conclude from the warming at MAR_0 that the whole of AABW is warming, the deepest instruments on MAR_1 also showed a warming (on the order of 0.015°C). The warming at both locations may be due to a zonal repositioning of the sloping isotherms between MAR_0 and the ridge, but it is also consistent with a longer term warming trend.

Comparing the data to the nearest hydrographic casts (Fig. 5a), we see that the $\theta - S$ range at WB_6 lies most closely along the 2010 profile and that the warm, salty fluctuations are along the $\theta - S$ curve rather than a shift in the $\theta - S$ relationship. Variance in temperature and salinity are plotted as ellipses along the major and minor axes of variability following Emery and Thompson, 2004 [@]. At MAR_0, the 1981 casts were colder and saltier than both the more recent casts and the mooring data, even including variability given by the standard deviations of temperature and salinity (Fig. 5b). The long term warming from hydrography, both at WB_6 and MAR_0 is stronger than the short-term variability observed at the mooring sites.

3.2. AABW transport variability

Overall, the range in transports over the six-month period, below 4100 dbar, was 1 to 3 Sverdrups, with a standard deviation of 0.4 Sv (Fig. 6). Comparing this to the previous decades, the range is larger over the six month deployment than between the six hydrographic sections, where transport ranged from 2.2 to 3.7 Sv (Table 1) though the mean is smaller. Note that the AABW transport estimates from hydrography in Table 1 are calculated differently than in the later section on hydrography where only water colder than 1.8°C will be included. For comparison with the moorings, where the transport cannot be partitioned by temperature, the values in Table 1 include all water below 4100 dbar.

Transport variability is dominated by changes at the deepest instruments on WB_5 in the western boundary. These transports have been estimated for the overlap period between WB_6 and MAR_0, from Apr–Nov 2009 using transport profiles which have been extrapolated to zero below 5600 dbar. There were several increases in transport—which peaked at the beginning of May, mid-June, and the beginning of August—that corresponded to increases in temperature at WB_6 (Fig. 4a). There was also a large increase in transport in the last month (November) resulting from a general warming in the upper layers near the bottom of WB_5. The gradual warming at both MAR_0 and MAR_1 results in a slow decline of AABW transport (until the November reversal).

Transport profiles between 70.5°W and 49°W are shown in Fig. 7. Profiles have been averaged by month and the profiles calculated from the nearest hydrographic stations in 1981, 2009 (calibration casts) and 2010 are shown as well. The figure includes April through October, with November having been omitted as short (<2 weeks). The structure and magnitude of transport profiles in the seven month mooring period matches the previous estimates. However, the local bottom depth at WB_6 and MAR_0 is at 5600 dbar. Transport per unit depth estimates from hydrography (§4.3) show that, for example, in 2010, 0.6 Sv or 20% of the AABW transport was located below 5600 dbar. In addition, the transport between 49°W and 46°W is neglected. However, from the transport estimates between these two longitudes from hydrography (Table 1), we can see that this contribution is very small or nil.

4. Results: Hydrographic sections

4.1. AABW property changes across decades

The six hydrographic sections show similar overall structure and properties of AABW from 1957–2010 (See Fig. 2 and 3). The water below 4500 dbar is cold ($\theta < 1.9$°C) and relatively fresh ($S \sim 34.89$) compared with the overlying NADW ($\theta > 1.9$°C and $S > 34.899$). Comparing the sections, the contour choice highlights the change in the coldest watermasses: in 1957, no water colder than 1.5°C was measured (Fig. 2). The volume of water colder than 1.5°C increased from nothing in 1957 to its peak in 1992 before its near absence in 2010. This suggests that the volume of coldest AABW at 24°N has fluctuated.

By comparing the cross-sectional area of water colder than a particular isotherm, we can compare variations in volume between years (Fig. 8). The particular trends apparent are that below 1.54°C, 1992 had the largest volume (estimated from cross-sectional area) of water which decreased monotonically through the 1998, 2004 and 2010 sections. However, at warmer isotherms, e.g., 1.7°, the pattern is not the same. The volume of water colder than 1.7°C was greatest in 1998, and somewhat less in subsequent sections. If we look at total AABW volume, defined as water colder than 1.8°C (following Johnson et al., 2008 [@]; Lavin et al., 2003 [@]), the most recent three sections, including 2010, had the largest volume of water. These changes indicate that rather than an overall contraction of AABW volume at 24.5°N, the properties of AABW have shifted towards a slightly warmer mean temperature with a decrease in the volume of water colder than 1.5° since 1992, but a larger overall volume of water colder than 1.8° since 1998.

4.2. AABW structure and volume

AABW, as delineated by the 1.8°C, has isotherms that slope up from 70°W to 55°W, then deepening towards the MAR (see Fig. 9a). By the thermal wind relationship, the upwards slope to the east is indicative of northward flow below. West of 70°W, isotherms follow bathymetry. The slope of the isotherms has zonal structure that persists in all six sections. From 70°W to 66°W, the slope is steepest, indicative of faster northward flow. From 66°W to 61°W, isotherms are nearly level, before they shoal again from 61°W to 52°W. This temperature structure follows structure of the bathymetry north of 24°N where a submarine ridge divides the deep western basin into a small basin to the west, and the larger basin to the east (See Fig. 1). The pattern of slopes in isotherms suggest a northward flow at the MAR, southward recirculation around 66–61°W, and northward circulation between 70° and 66°W.

In addition, there appear to be small-scale—possibly eddy—features. In the 2004 section, there is a localized shoaling of isotherms at 70°W. Considering the slope of isotherms from the western endpoint of AABW to 46°W, the basin-wide slope is reduced for a western end point of 70°W, in an eddy and relatively enhanced for 70.5°W. Since eddy features are likely to be transient, and not necessarily representative of large-scale changes in AABW transport, we avoid integrating transports from an end point within an eddy and use a western integration limit of 70.5°W rather than 70°W.

The core of AABW (as given by the coldest temperatures measured at 5990 dbar, the deepest measurements common to all six sections) also changes position from section to section. Most years, the core is betwee 58.8–57.8°W except in 1957 and 2010 when it moved west to around 61°W (not shown). The vertical structure of temperature and salinity at the core stations reveals a large volume of weakly stratified water below about 5200 dbar with a thermocline above. Temperatures in the most recent three sections warm more rapidly in the thermocline with distance from the bottom. Salinities shift more gradually between occupations, showing some variation in the most recent three sections. A small but progressively warming and salinification of the deep, weakly stratified layer is apparent from 1998–2010.

The $\theta - S$ profiles from the core stations are shown in Fig. 10. Very little variation is apparent in the most recent three sections except that the extreme of the coldest, freshest range is progressively disappearing. Again, the 2010 hydrographic section shows the absence of coldest, freshest water.

The pattern of change between sections is shown in Fig. 11. Note that the latitude of sections deviated at the western boundary and the mid-Atlantic ridge (Fig. 1c); early sections were along a single latitude, 24.5°N while later sections connected with the Florida Straits in the west (26.5°N). Temperature comparisons in the western basin are only valid east of 68°W. Johnson et al., 2008 [@] described a pattern of warming and cooling that indicated a decrease in the tilt of the isotherms between the 1981 to 2004 section (Fig. 11a). This pattern was not continued in 2010. Instead, since 2004, the entire volume of AABW below 5500 dbar has warmed (below the average position of the 1.6°C isotherm, while above 4000 dbar or the 2.0°C, the water has warmed. Between 4000 and 5500 dbar, the region between 65 and 68°W and between 55–50°W has warmed, and between the two has cooled. These changes will work to decrease the recirculation noted above, smoothing the isotherm depth in 2010 (as can be seen in Fig. 9a). From 1981–2010, above the 2°C isotherm, the region east of 60°W has warmed, while west of 60°W has cooled. These changes will affect shear in the NADW layers, but due to our choice of reference level at 4100 dbar, will not project onto AABW transport estimates here. The total effect since 1981 has been a warming of the deepest layers of AABW (below 5500 dbar) and a cooling of the water below 4100 dbar.

4.3. AABW transport across decades

The relative strength of AABW transport from the six hydrographic sections is mostly insensitive to the choice of longitudinal limits or reference level. The zonally-integrated transport of water colder than 1.8°C from 46°W to a variable western longitude limit, and relative to a reference level of 3200 or 4100 dbar is shown in Fig. 12a and b, respectively. The x-axis represents the western limit of integration. From this we can see that for any western limit and either reference level, 1981 had the highest northward transport of AABW. Note that the values change slowly in most cases for a given year and have varying longitude limits. Two exceptions are the localized dips in transport for 1981 at 71°W and for 2004 at 70°W. These may be local transient eddies which deflect isotherms and would then not be representative of the overall transports. The range between 1981 and 2004 transports is larger when using a 3200 dbar reference level. Additionally, using the reference level of 3200 dbar, the magnitude of reduction in AABW transport from 1981 to 2004 was accentuated by the particular choice of western longitudinal limits from Johnson et al., 2008 [@]. However, with few exceptions, the monotonic reducing trend in transports between 1981 and 2004 is apparent regardless of the choice of longitudinal limits or reference level.

Similarly, for both reference levels and a range of longitudinal limits, the transport in 2010 of water colder than 1.8°C is similar to that observed in 1998, and about average for all the sections except for 1981. For our choice of a 4100 dbar reference level and a 70.5°W west limit, while total transport decreased monotonically from 1981 (3.7 Sv) to 2004 (2.4 Sv), there was a resurgence of AABW in 2010 (2.8 Sv), giving an overall mean value of 2.8 for the six sections and standard deviation of 0.6 Sv.

5. Discussion

From hydrographic sections between 1957 and 2010, and continuous mooring records in 2008–2009, we have estimated transport and property changes in AABW at 24.5N in the Atlantic. The coldest core of AABW (found between 57°W and 61°W) has warmed since 1992; while the overall volume of AABW has not changed, the coldest vintages have disappeared. A similar warming trend was observed in the mooring records, consistent with the recent global warming of AABW estimated from hydrographic sections in Purkey and Johnson, 2010 [@], in the South Atlantic [Johnson and Doney, 2006, @] and through the Vema channel [Zenk and Morozov, 2007, @].

There're two main distinctions between our analysis of the mooring data and the hydrographic data. Moorings allow us to observe the variability in transport on short time scales which has been shown to be important both in the RAPID project as a whole and now here for AABW. The ranges in transport estimated are large (2 Sv) and on the order of the range estimated from hydrographic sections. However, mooring data is spatially sparse and in this instance resulted in an estimate of AABW as the net northward transport below 4100 dbar and between 70.5–49°W. Hydrographic data allow a more natural estimate of AABW delineated by density or temperature (used here). In comparing the two estimates (below 4100 dbar) and colder than 1.8°C from hydrography, we see that our estimate of transport below 4100 dbar contracts the variability observed when using the full temperature data. (Table 1: column 1 shows a transport range of 2.2–3.7 Sv vs Fig. 9b which gives a range of 1.9–4 Sv.) This would suggest that our mooring estimate of AABW transport is actually an underestimate of the true variability.

On comparing properties of AABW, the hydrographic data are superior. The short term variability in temperature from moorings is responsible for the fluctuations observed in transport, but it is difficult to conclude anything from the warming trend observed near the bottom at the MAR moorings. Without further information, the warming signal could be due to a movement in the isotherms delineating AABW or a change in the bulk properties of AABW. In contrast, the warming signal from hydrographic sections is robust and shows that indeed, the deepest, coldest classes of AABW have been warming since 1981 though the volume of water colder than 1.8°C has increased.

The warming observed both globally and in this observations may be due to a change in the source waters of AABW or in advection and mixing along the path from the source regions to 24°N. Near the source, recent results have suggested that the export of AABW from the Weddell Sea has been changing: the coldest waters are no longer being exported, possibly due to a localised bottom Ekman effect [Jullion et al., 2010, @; Meredith et al., 2011, @]. Understanding changes along the path from the Southern Ocean is more difficult. If transport speeds were to slow, then the observed warming at more northerly latitudes may have resulted from the longer advective timescales which would allow for more mixing with warmer NADW along the pathway. Clearly, rates of transport are better identified using moorings, in order to capture the time variability of the process, but the short term variability observed by the six month mooring deployment may not be long enough to infer changes due to processes along the pathway from the Southern Ocean.

One of the motivations for calculating AABW transport variability was to understand its impact on estimates of the MOC at 26°N in the RAPID array. The current RAPID-WATCH calculation assumes a near steady 2 Sv of northward flowing AABW, peaking at 5500 dbar [Kanzow et al., 2010, @]. Based on the estimates here, the true value may range from 1 to 5 Sv. If the nominal 2 Sv transport currently used in the RAPID estimate of the MOC overturning were reduced to 1 Sv, the estimate of MOC overturning would increase by 0.2 Sv, transferring about 20% of the variability. If the AABW transport were increased to 5 Sv, the MOC overturning estimate would reduce by 0.6 Sv. While a 0.8

Sv range is within the error estimates for the MOC calculation, it is of the same order as other uncertainties now being quantified.

The balance between the upper and lower MOC cells has been explored in modeling and paleo studies, which suggest a seesaw pattern of dominance shifting between northern hemisphere deep water sources (upper cell) and AABW (lower cell). However, global models are poorly constrained in the deep ocean due to a lack of observations [Saunders et al., 2008, @]. Besides allowing a direct estimate of deep transport at 26°N, these deep moorings will provide temperatures, salinities and currents which can be used to improve models in their deepest layers.

Acknowledgments. The RAPID-WATCH MOC monitoring project is funded by the Natural Environment Research Council (NERC). Data are freely available from http://www.noc.soton.ac.uk/rapidmoc. The MOCHA project is funded by the National Science Foundation (NSF). The authors would like to thank W. Johns, S. Elipot, J. J-M. Hirschi and L. Juillon for helpful discussions. Special thanks to the captain, crew and science parties involved in the hydrographic section and RAPID/MOCHA mooring deployment and recovery.

References

Bryden, H. L., Longworth, H. R., and Cunningham, S. A. (2005). Slowing of the Atlantic meridional overturning circulation at 25°N. *Nature*, 438:655–657.

Bryden, H. L., Mujahid, A., Cunningham, S. A., and Kanzow, T. (2009). Adjustment of the basin-scale circulation at 26°N to variations in Gulf Stream, deep western boundary current and Ekman transports as observed by the RAPID array. *Ocean Science*, 5:421–

433.

Cunningham, S. A., Kanzow, T., Rayner, D., Baringer, M. O., Johns, W. E., Marotzke, J., Longworth, H. R., Grant, E. M., Hirschi, J. J.-M., Beal, L. M., Meinen, C. S., and Bryden, H. L. (2007). Temporal variability of the Atlantic meridional overturning circulation at 26.5°N. *Science*, 317:935–938.

Emery, W. J. and Thompson, R. E. (2004). *Data Analysis Methods in Physical Oceanography.* Elsevier, San Diego, 2nd and revised edition.

Johns, W. E., Beal, L. M., Baringer, M. O., Molina, J. R., Cunningham, S. A., Kanzow, T., and Rayner, D. (2008). Variability of shallow and deep western boundary currents off the Bahamas during 2004–05: Results from the 26°N RAPID–MOC array. *Journal of Physical Oceanography*, 38:605–623.

Johnson, G. C., and Doney, S. C. (2006). Recent western south Atlantic bottom water warming. *Geophysical Research Letters*, 33:L14614.

Johnson, G. C., Purkey, S. G., and Toole, J. M. (2008). Reduced Antarctic meridional overturning circulation reaches the North Atlantic Ocean. *Geophysical Research Letters*, 35:L22601.

Jullion, L., Jones, S. C., Naveira Garabato, A. C., Meridith, M. P. (2010). Wind-controlled export of Antarctic Bottom Water from the Weddell Sea. *Geophysical Research Letters*, 37:L09609.

Kanzow, T., Cunningham, S. A., Johns, W. E., Hirschi, J. J.-M., Marotzke, J., Baringer, M. O., Meinen, C. S., Chidichimo, M. P., Atkinson, C., Beal, L. M., Bryden, H. L., and Collins, J. (2010). Seasonal variability of the Atlantic meridional overturning circulation at 26.5°N. *Journal of Climate.*

King, B. A. (2011). RRS Discovery Cruise 346, Jan–Feb 2010. A transatlantic hydrography section at 24.5°N. *National Oceanography Centre Southampton Cruise Report, XX*, Southampton, UK.

Lavin, A. M., Bryden, H. L., and Parrilla, G. (1998). Meridional transport and heat flux variations in the subtropical North Atlantic. *The Global Atmosphere and Ocean System*, 6:269–293.

Lavin, A. M., Bryden, H. L., and Parrilla, G. (2003). Mechanisms of heat, freshwater, oxygen and nutrient transports and budgets at 24.5°N in the subtropical North Atlantic. *Deep Sea Research*, 50:1099–1128.

Limeburner, R., Whitehead, J. A., and Cenedese, C. (2005). Variability of Antarctic Bottom Water flow into the North Atlantic. *Deep Sea Research*, 52:495–512.

Meredith, M. P., Gordon, A. L., Naveira Garabato, A. C., Abrahamsen, E. P., Huber, B. A., Jullion, L., and Venebles, H. J. (2011). Synchronous intensification and warming of the Antarctic Bottom Water outflow from the Weddell Gyre. *Geophysical Research Letters*, 38:L03603.

Orsi, A. H., Johnson, G. C., and Bullister, J. L. (1999). Circulation, mixing, and production of Antarctic Bottom Water. *Progress in Oceanography*, 43:55–109.

Purkey, S. G. and Johnson, G. C. (2010). Warming of global abyssal and deep Southern Ocean waters between the 1990s and 2000s: Contributions to global heat and sea level rise budgets. *Journal of Climate*.

Rayner, D., Hirschi, J. J-M., Kanzow, T., Johns, W. E., Cunningham, S. A., Wright, P. G., Frajka-Williams, E., Bryden, H. L., Meinen, C. S., Baringer, M. O., Marotzke, J., and Beal, L. M. (2011). Monitoring the Atlantic meridional overturning circulation.

Deep Sea Research II.

Saunders, P. M., Cunningham, S. A., de Cuevas, B. A., and Coward, A. C. (2008). Decadal changes in the North Atlantic and Pacific meridional overturning circulation and heat flux. *Journal of Physical Oceanography*, 38:2104–2107.

Trenberth, K. E. and Caron, J. M. (2001). Estimates of meridional atmosphere and ocean heat transports. *Journal of Climate*, 14:3433–3443.

U. S. Department of Commerce, National Oceanic and Atmospheric Administration, N.G.D.C. (2006). 2-minute gridded global relief data (etopo2v2).

Zenk, W. and Morozov, E. (2007). Decadal warming of the coldest Antarctic Bottom Water flow through the Vema Channel. *Geophysical Research Letters*, 34:L14607.

Table 1. Deep transport estimates from hydrographic sections between longitude pairs. Transports are calculated as a zonal-integral of geostrophic shear referenced to 4100 dbar between the nearest stations to each mooring longitude. Unlike the transport estimates in Fig. 9b which only considers transport of water colder than 1.8°C, these estimates are for total transport below 4100 dbar. Transports in this table are for comparison with the mooring data, which cannot be limited to water colder than 1.8°C.

	70.5–46°W WB_6 to 46°W [Sv]	70.5–49°W WB_6 to MAR_1 [Sv]	49–46°W MAR_1 to 46°W [Sv]
1957	2.2	2.2	0.0
1981	3.7	4.0	-0.3
1992	3.2	3.2	0.0
1998	2.6	2.6	0.0
2004	2.6	2.6	0.0
2010	2.5	2.4	0.1
	2.8±0.6	2.8±0.7	0.0±0.1

Table 2. Hydrographic Sections, number of stations that are east of 77°W and the mean and standard deviation of distance between stations.

Year	Ship	Dates	Stations [#]	Spacing [km]
1957	RRS *Discovery II*	6–28 Oct	38	162±48
1981	RV *Atlantis*	12 Aug–6 Sep	90	71±31
1992	BIO *Hespérides*	20 Jul–16 Aug	101	61±13
1998	RV *Ronald H. Brown*	23 Jan–24 Feb	121	55±23
2004	RRS *Discovery*	4 Apr–10 May	113	59±26
2010	RRS *Discovery*	5 Jan–19 Feb	122	55±23

Table 3. Ekman, Florida Current and Bering Strait transports used for mass balance in the hydrographic sections. Ekman and Florida Current transports for 2010 were the average values from 2008. The barotropic velocity column is the amount of barotropic velocity which was necessary to apply west of 70.5°W in order to achieve mass balance across the section.

	Ekman [Sv]	Florida Current [Sv]	Bering Strait [Sv]	barotropic [cm s^{-1}]
1957	4.5	31.1	-0.8	0.0
1981	3.7	31.1	-0.8	-0.2
1992	4.6	30.3	-0.8	1.7
1998	5.2	34.0	-0.8	-0.4
2004	4.5	31.8	-0.8	0.2
2010	4.1	31.6	-0.8	-0.3

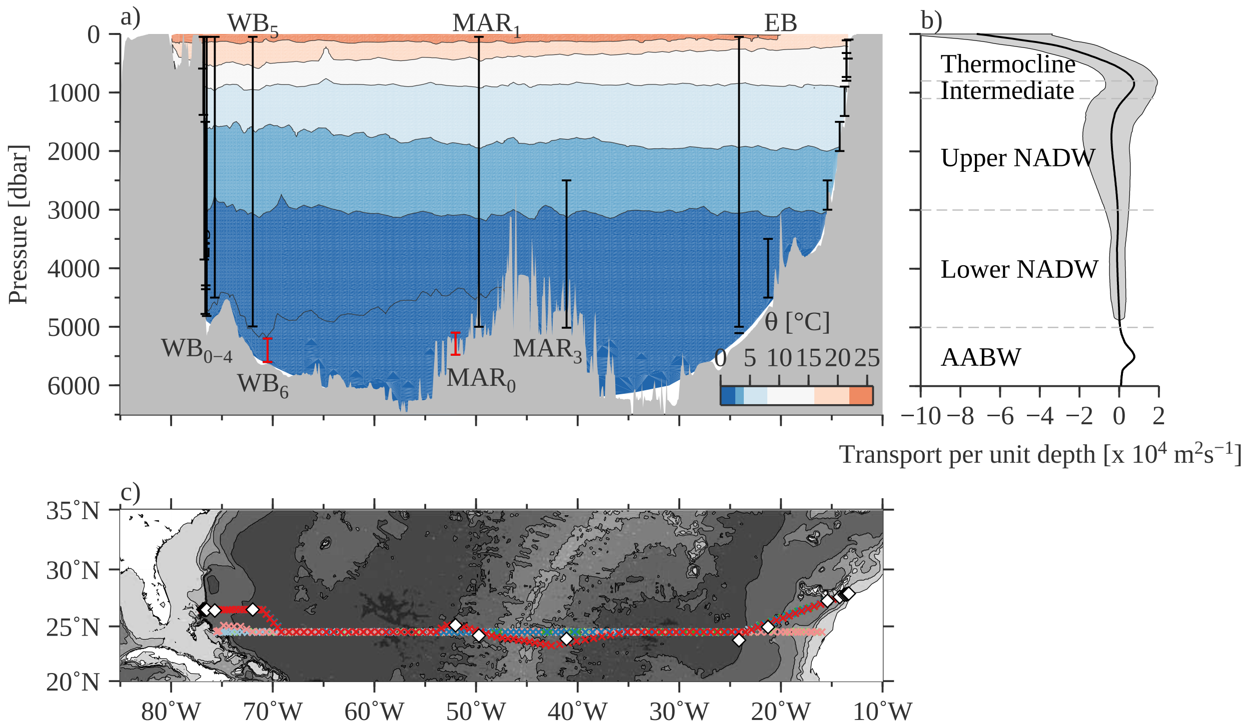

Figure 1. Array setup at 24–27°N in the Atlantic. (a) Potential temperature at 26°N in the Atlantic from the 2010 occupation of the line. Mooring locations from the RAPID-WATCH/MOCHA program are given by the vertical lines. The two red vertical lines highlight the deep moorings added for this study: in the abyss at 70.5°W (WB$_6$) and 52°W (MAR$_0$). (b) Transport per unit depth east of the Bahamas calculated from the moorings. The solid thick line is the mean while shading indicates the standard deviation between April 2004 and March 2009. The shear is divided into major water mass classes, including thermocline water, Antarctic Intermediate Water, North Atlantic Deep Water and Antarctic Bottom Water. (c) Bathymetry around 20–35°N and station positions for six occupations of the hydrographic section, in 1957 (pale green), 1981 (light blue), 1992 (pink), 1998 (green), 2004 (dark blue) and 2010 (red). Mooring positions are given by white diamonds. Note, the 2004 and 2010 sections follow the same track except for near the mid-Atlantic ridge. 1957 and 1981 are across 24.5°N, as is 1992, with the exception of a deviation near the western boundary.

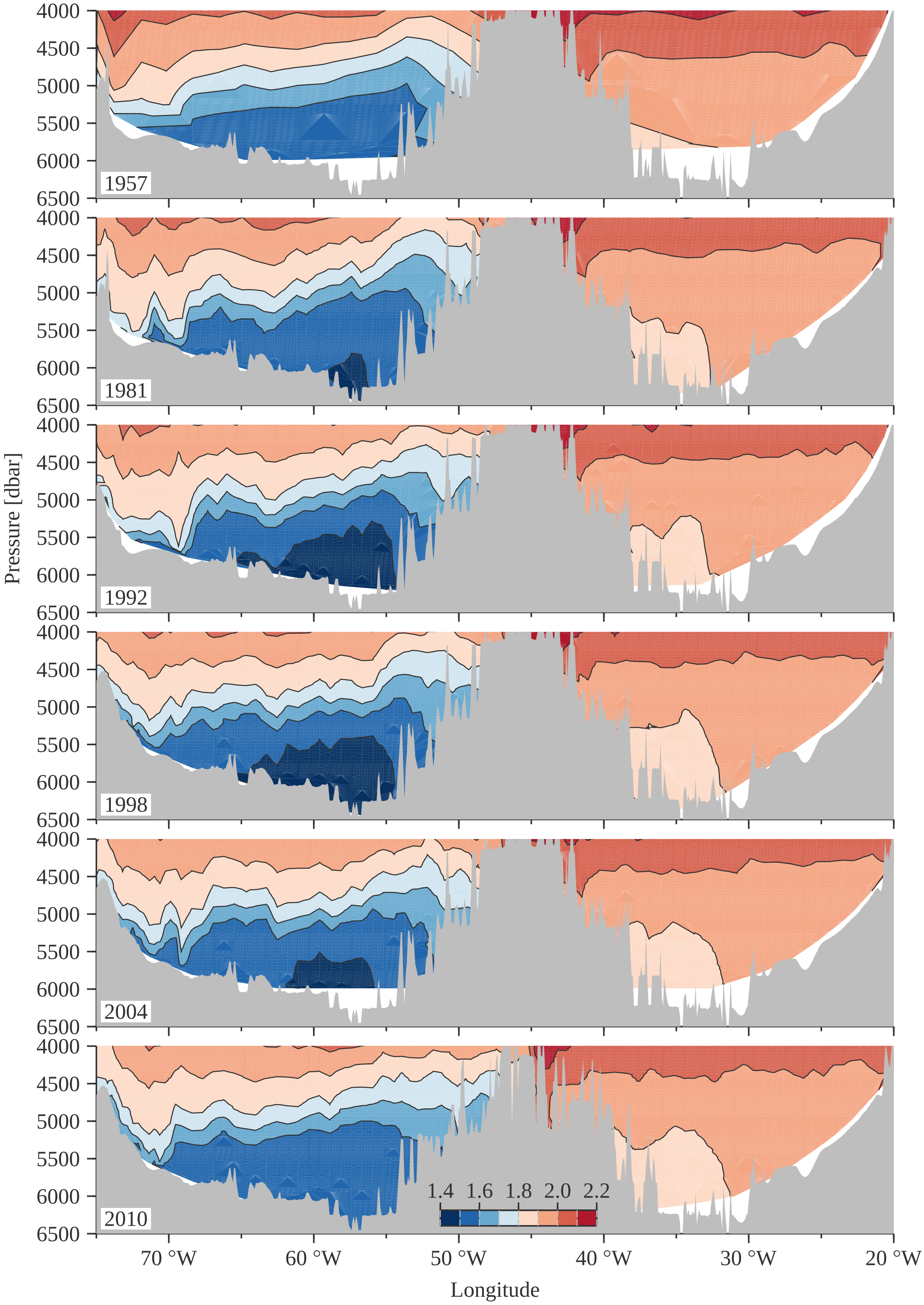

Figure 2. Deep potential temperature sections from the six hydrographic cruises at 24.5–26.5°N in the Atlantic. Contours of potential temperature are at 0.1°C intervals. Bathymetry is shaded and represents the bottom depth from ETOPO along each the hydrographic section.

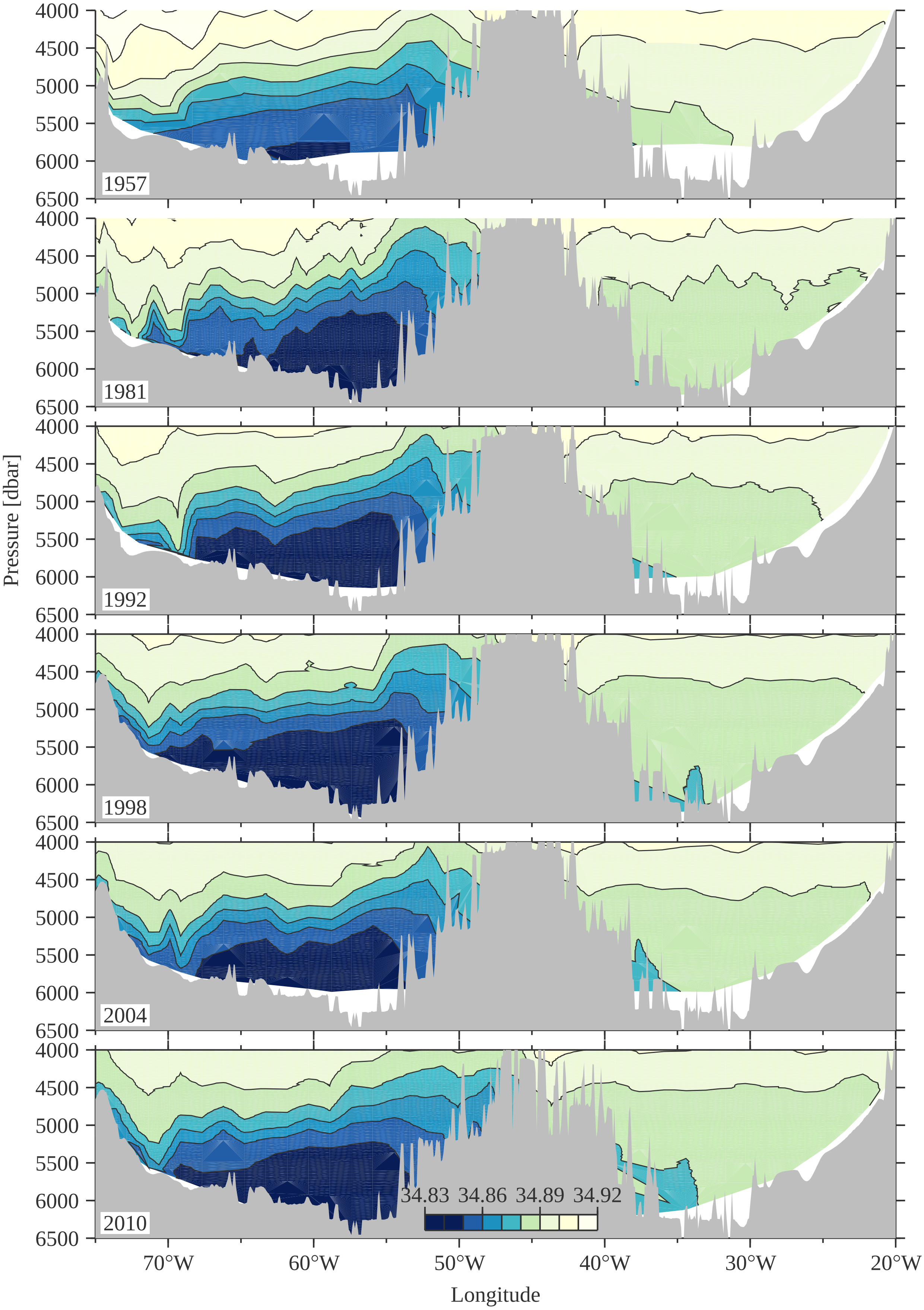

Figure 3. Deep salinity sections from the six hydrographic cruises at 24.5–26.5°N in the Atlantic. Contours of salinity are at 0.01 intervals. Bathymetry is shaded and represents the bottom depth from ETOPO along each the hydrographic section.

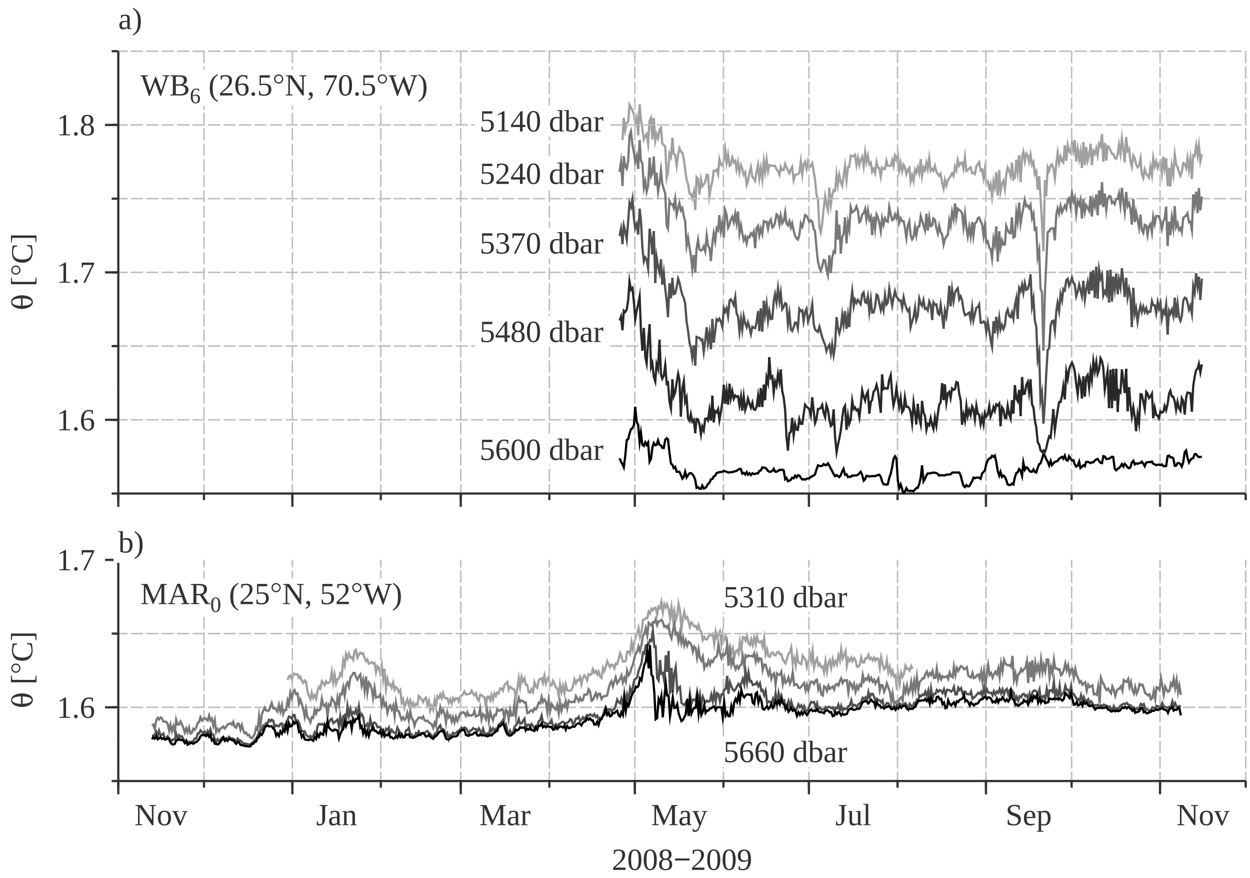

Figure 4. Potential temperature from WB_6 (a) and MAR_0 (b) from each moored MicroCat. Pressure annotated are approximate averages for each record from WB_6 and the range for the four instruments on MAR_0 (5310, 4330, 5580 and 5660 dbar). Instruments were spaced at 100 dbar intervals. Data have been calibrated and subsampled to 12 hourly intervals.

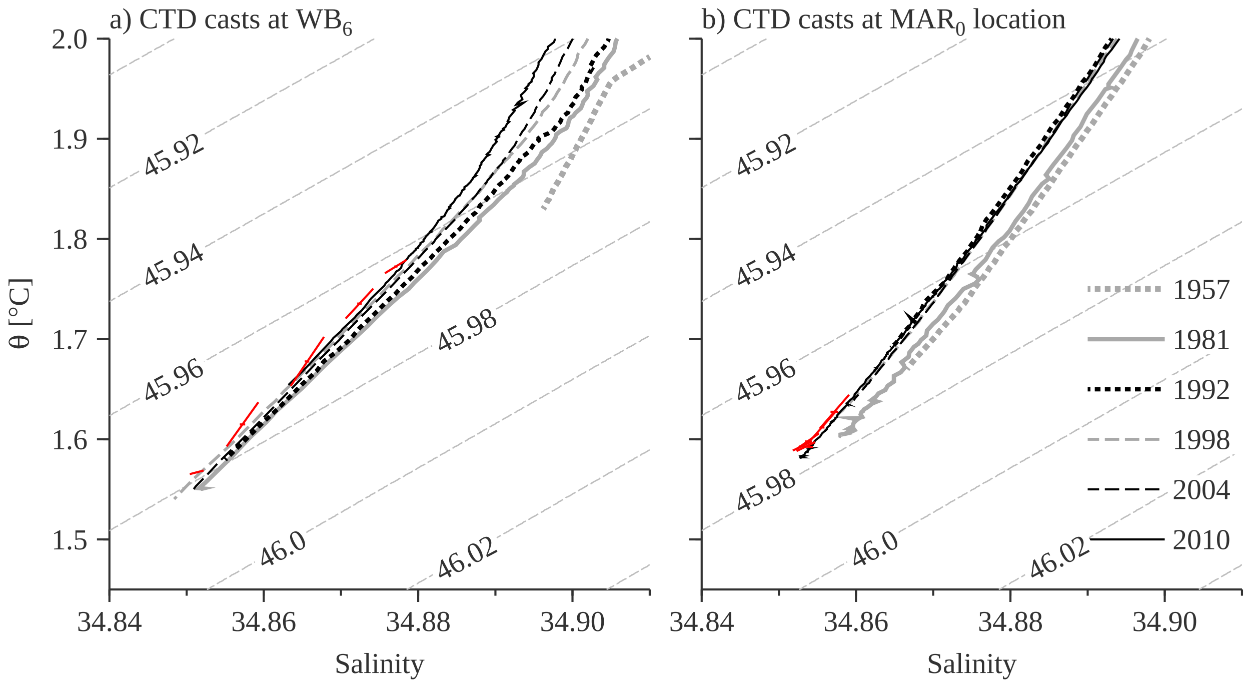

Figure 5. Temperature and salinity from the six hydrographic sections at the two deep mooring sites, (a) WB_6 and (b) MAR_0. Temperatures and salinities from the mooring deployments are given by the red crosses, where the axes are standard deviations along the major and minor axes of variance ellipses. Potential density (σ_4) is contoured.

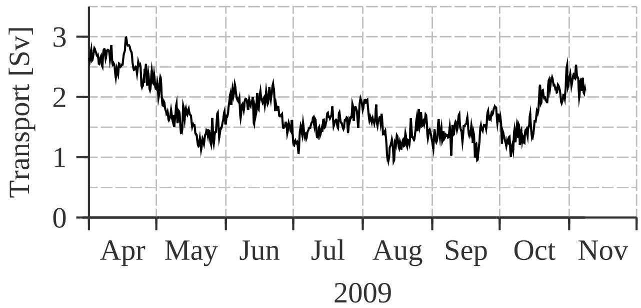

Figure 6. Net transport below 4100 dbar between 70.5 and 49°W estimated from mooring data over the period where the WB_6 and MAR_0 deployments coincided. Below the deepest common level (5600 dbar), each transport profile has been been extrapolated to zero at 6300 dbar.

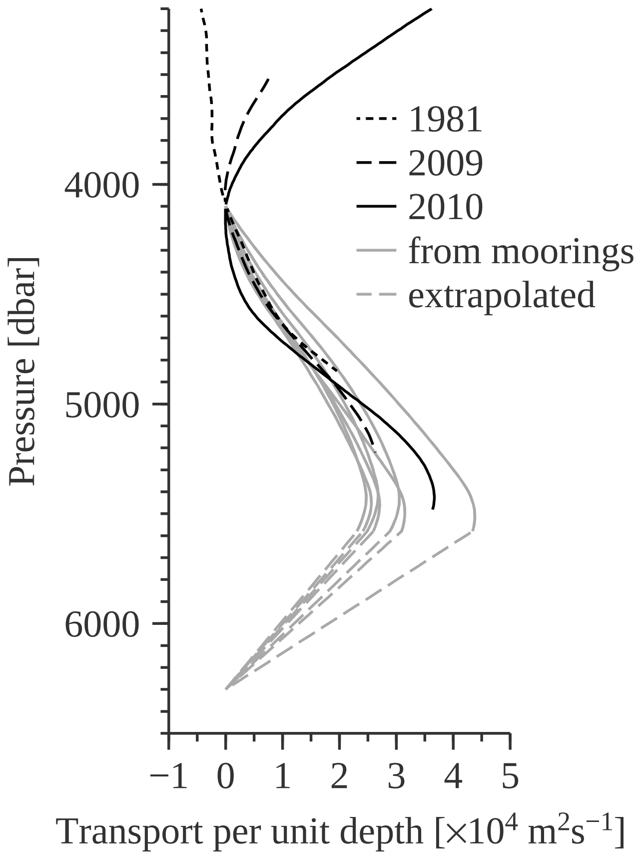

Figure 7. Transport profiles from moorings (gray) and hydrography (black) between 70.5 and 49°W, relative to a level-of-no-motion at 4100 dbar. Hydrographic data from 2009 is from CTD casts during the mooring deployment cruise. Estimates from hydrographic data use the shear between the stations nearest the mooring locations, so transport estimates are limited to the depth range above the deepest common level between the two stations. Mooring transport estimates are averaged by month (April–October, November having been omitted since the record is short). Dashed gray lines show transports linearly extrapolated to zero the 6300 dbar.

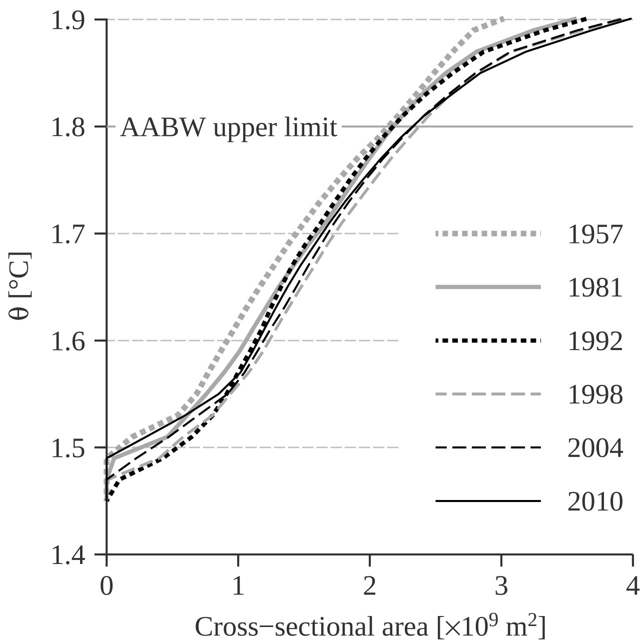

Figure 8. Cumulative volume of water colder than a given temperature estimated as a cross-sectional area across 24.5°N between 77 and 20°W from hydrographic sections. Before estimating volume, station data were gridded onto a fine pressure–longitude grid and the bottom of each profile was filled by continuing the deepest measurement down to bathymetry estimates across 24.5°. Using bathymetry at 24.5°N rather than at station positions reduces differences in volume estimates due to varying cruise track positions. Water colder than 1.8°C is called AABW.

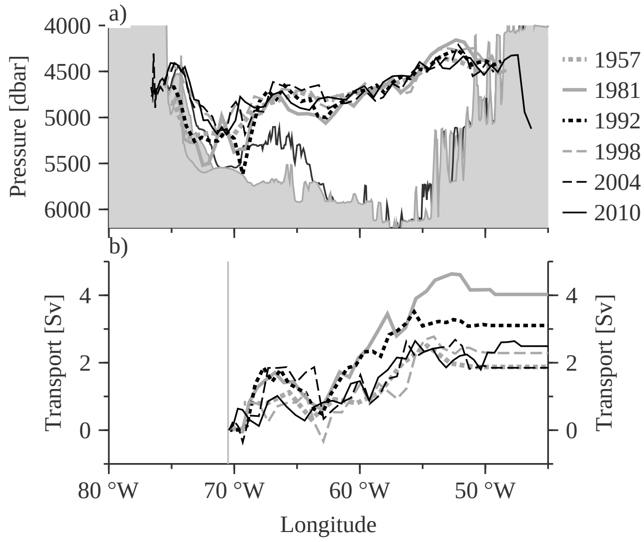

Figure 9. a) Depth of the 1.8°C isotherm (in dbar) from the six hydrographic sections. The bathymetry at 24.5°N is shaded in light gray. The bathymetry at 27°N is shaded in the hachure pattern. Note the elevated bathymetry around 65-70°W. (b) Cumulative transport of AABW (water with $\theta < 1.8$°C) from the hydrographic sections, integrated from zero at 70.5°W to the east.

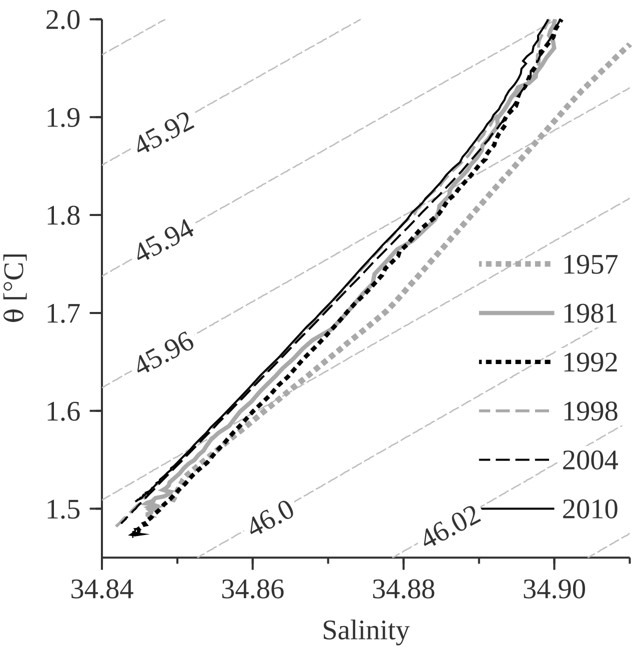

Figure 10. $\theta - S$ plot from the coldest core of AABW for each hydrographic section. Contours are potential density referenced to 4000 dbar (σ_4).

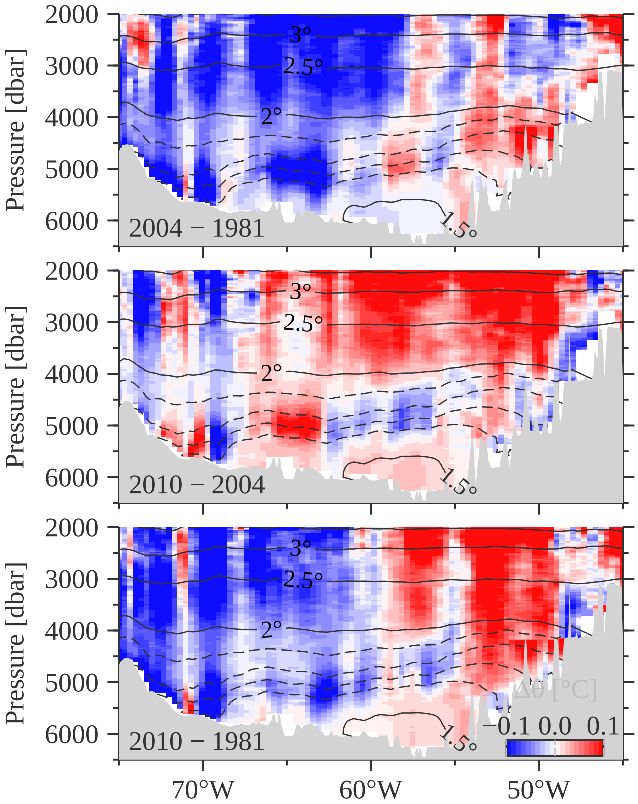

Figure 11. Temperature changes between (a) 1981 and 2004, (b) 2004 and 2010, and (c) 1981 and 2010, calculated as modern minus older. Red regions indicate warming while blue regions indicate cooling. Temperatures were first gridded for each hydrographic section data onto a fine pressure–longitude grid before differencing. Isotherms contoured are the mean isotherm depths (in dbar) from the sections 1981, 1992, 1998, 2004 and 2010 at 0.5° intervals in solid black, and between 1.5–2.0°C at 0.1° intervals in dashed black.

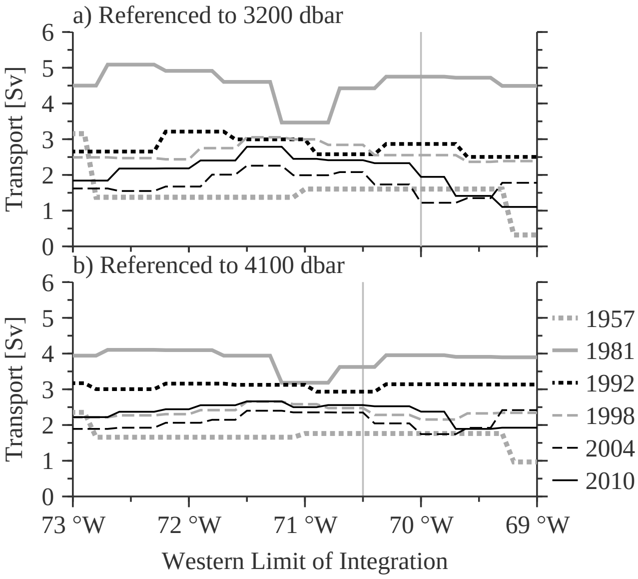

Figure 12. Effect of choice of reference level and longitude limits on AABW transport estimate. (a) The zonal integral of transport from 46°W to the western limit of integration (x-axis), referencing geostrophic velocity to 3200 dbar. The vertical line is the western limit used in Johnson et al., 2008 [@]. (b) The same as in (a) except referencing geostrophic velocity to 4100 dbar. The vertical line is the western limit used here.